



# The vertical structure of mesoscale eddies in the Azores Current

# 2 corridor: a combined altimetry-ARGO analysis

- 3 Susana M. Silva-Fernandes<sup>1</sup> and Álvaro J. Peliz<sup>1</sup>
- 4 <sup>1</sup>Instituto Dom Luiz Faculdade de Ciências, Universidade de Lisboa, Lisboa, Portugal
- 5 Correspondence to: Susana Margarida Silva-Fernandes (smsilva@fc.ul.pt)
- 6 Abstract. Temperature and salinity, derived from over 20000 Argo profiles, are combined with 20 years of eddy trajectories 7 and absolute dynamic topography maps to characterise the vertical structure of mesoscale eddies within the Azores current 8 corridor (AzCCo) from surface to 1500 dbar. The isopycnal decomposition temperature and salinity anomalies into two 9 components – heave (HEV) (vertical deflection of isopycnal surfaces) and spice (SPI) (variation along an isopycnal surface) 10 - are directly associated with two main eddy transport mechanisms: eddy pumping and eddy trapping. From east to west, our statistics reveal an intensification of the anomalies' maximum (from 0.5° C and 0.1 to above 1.5° C and 0.2 of salinity) and a 11 deepening of their core location in the water column (from 250 dbar to 750 dbar) for both anticyclones and cyclones. 12 13 Furthermore, the absolute values of isopycnal vertical displacement above 50 dbar, from the surface to the 1500 dbar level, 14 demonstrate the significant impact of these mesoscale structures throughout the water column. Anticyclones are characterised 15 by a more barotropic structure, exhibiting warm, salty cores, while cyclones demonstrate a more baroclinic structure, featuring cold, fresh cores along the AzCCo. The origins of the sampled eddies can explain the zonal differences in vertical structure on 16 17 either side of the Mid-Atlantic Ridge (MAR). In the west, most eddies could originate from the Gulf Stream branches, resulting 18 in higher anomaly values to the west of the MAR. The HEV process dominates the resulting vertical structures of temperature 19 and salinity within the water column. SPI exhibits higher values within the upper 250 dbar to the east of the MAR, reflecting 20 an eddy's tendency to trap different water masses at the surface. The dominance of HEV indicates that most eddy-induced anomalies originate from eddy pumping, which is manifested as deflections of isopycnal surfaces. This mechanism produces 21 22 warmer, saltier anomalies within anticyclonic eddies due to downwelling of isopycnal surfaces and colder, fresher anomalies 23 within cyclonic eddies due to upwelling of the same surfaces.

#### 1 Introduction

- Mesoscale eddies play a crucial role in redistributing heat, salt, and momentum (e.g., Chelton et al., 2011; Treguier et al., 2012;
- Dong et al., 2014; Frenger et al., 2015) by the advection of water masses with distinct thermohaline properties (eddy trapping)
- 27 from their formation regions to their dissipation sites. In addition, vertical motions induced by mesoscale structures (eddy
- 28 pumping) influence the transport of nutrients within the water column, while their rotational flow modulates the horizontal
- distribution of chlorophyll and phytoplankton concentrations (e.g., Martin and Richards, 2001; Gaube et al., 2011; Mahadevan,
- 30 2016; Keppler et al., 2024).



31

3233

34

35

36

37

38

39

40

41 42

43

44

45

46 47

48

49

50

5152

53

54

55

56

5758

59

60

61 62

63

at 770 dbar.



The Azores current (AzC) is a highly turbulent zonal jet located around 34° N with mean eddy kinetic energy (EKE) values above 200 cm<sup>2</sup> s<sup>-2</sup> (Figure 1), the highest of the eastern subtropical North Atlantic. The current system and its associated frontal zone have been revisited several times over the last decades (e.g., Gould, 1985; Juliano and Alves, 2007; Frazão et al., 2022). The latitudinal band surrounding the jet, which we will loosely refer to as the Azores Current Corridor (AzCCo) is characterised by free eddies, meanders, and filaments, mostly evolving from baroclinic instability of the jet (Klein and Siedler, 1989; Alves and De Verdière, 1999) as well as several other types of structures propagating into the corridor. Different zonal sectors with distinct characteristics have been identified in the AzCCo, characterised by decreasing EKE values from west to east, which approximately coincide with the locations of two prominent topographic features in the area. Barbosa Aguiar et al. (2011) consider three main sectors: the western side between MAR and the Seewarte seamount chain (SWSM) (~28° W), the central area between 28° W and 20° W, and the eastern one spanning to the Gulf of Cadiz. While global statistics of the AzC surface eddy field are relatively well known (e.g. Barbosa Aguiar et al., 2011; Silva-Fernandes and Peliz, 2020), a systematic study of the internal structure of these eddies and their impact on the water column is still missing. Existing works comprise mainly isolated events derived from in situ data (e.g., Pingree et al., 1996; Pingree and Sinha, 1998; Mouriño et al., 2002; Mouriño et al., 2003), with most of these studies focusing on the large cyclonic eddies along the "Storm Corridor" (~ 34° N; Pingree, 2002). These large cold-core cyclones are characterised by horizontal temperature anomalies around 2.5° C between 200 and 600 dbar. With a core temperature as low as 3.5° C centred at the 400 dbar level. Also, Pingree et al. (1996) suggested that these eddies have vertical displacements of the isopycnal surfaces of around 200 dbar from the surface to near the bottom (4000 m). Pegliasco et al. (2015) characterised the vertical structure of two clusters of eddies using ARGO floats with origin in the Canary upwelling system, whose propagation to the west partially covers the AzCCo southern flank (west of 20° W). The surface cluster (with cores at around 0-200 m) has higher numbers of anticyclones detected inside our region with low positive anomaly values and short propagation trajectories, while the second cluster (eddies with maxima in the 200-600 m interval) presents more detected cyclones with anomalies of -0.5° C and -0.07 of salinity with a vertical extension down to 600-800 m. The cyclonic cluster reaches longitudes as far as 40° W (near the MAR), being part of the "Madeira corridor" (MdCo), previously coined by Sangrà et al., 2009 as the "Canary corridor". Finally, Amores et al. (2017) used composites of ARGO floats and altimetry (Sea Level Anomaly - SLA), covering part of the AzC southern flank (~32°N). They found peak anomalies around 150 m (anticyclones) and at 400-800 m (cyclones), reaching values of potential temperature above 1° C and 0.2 of salinity anomalies for both sign structures, although the cyclones were slightly more intense. Furthermore, the anticyclonic (cyclonic) eddies are generally characterised by warm (cold) and salty (fresher) cores, with their signals reaching a depth of 1200 m. West of the ridge, based on the trajectories of SOFAR floats launched on both sides of the MAR (Ollitrault and Colin de Verdière, 2002), reported that the eddies in that region have a southward flow south of 38° N, usually migrating along the west flank of the ridge. Furthermore, from the tracked eddies, they concluded that cyclones (anticyclones) have cold (warm) cores





Meddies are also encountered east of MAR, especially east of the SWSM and the Azores Plateau (AzP) (Bashmachnikov et al., 2015). As they travel west, their transport of Mediterranean water (MW) with high temperature and salinity (around the 800-1200 dbar levels) results in anomalies that can be easily tracked as they present temperature anomalies above 0.5° C and in salinity above 0.2 for a 200 m layer between 500 and 1500 m (Richardson et al., 1991; Bashmachnikov et al., 2015). Meddies are usually anticyclonic structures, but cyclone meddies are also found in our region of study, presenting vertical structures with high positive anomalies of temperature and salinity (lower than in anticyclonic meddies) and a vertical extension from 500 to 1300 dbar (Richardson et al., 2000; Barbosa Aguiar et al., 2013).

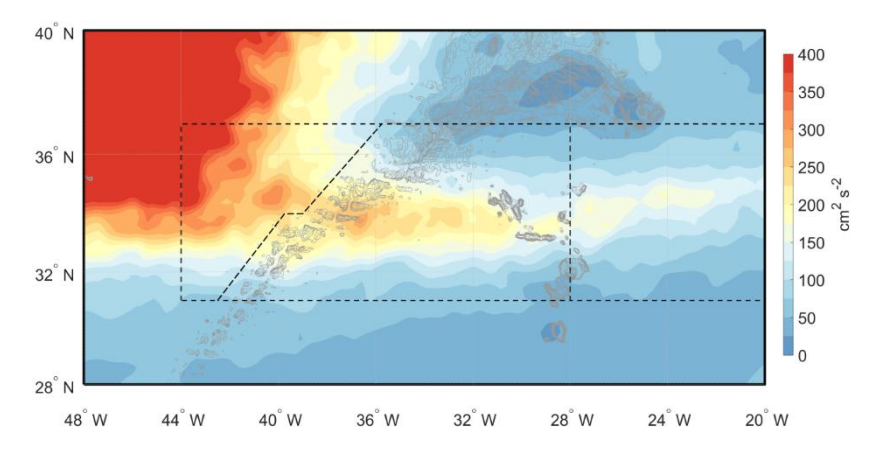


Figure 1: Map distribution of mean EKE (cm² s²) for the period 2005-2017. The three boxes represent the regions directly associated with the Azores Current Corridor: the eastern area R1, the central, R2, and the western one, R3. MAR - Mid Atlantic Ridge; SWSM - Seewarte seamount chain. The bathymetric lines are drawn every 500 m from the surface to 2500 m depth.

In this work, we analyse more than 20000 ARGO profiles combined with 20 years of altimetric data and an eddies' atlas (AVISO+, Sect. 2.3) to characterise the vertical structure of composite mesoscale eddies in the AzC corridor (AzCCo). Furthermore, we explore the concepts of Spice (SPI) and Heave (HEV), relating the observed variations in climatological temperature and salinity fields to eddy trapping, associated with the advection of distinct water masses, and eddy pumping, manifested as the deflection of isopycnal surfaces driven by the internal structure of anticyclonic and cyclonic eddies.

Therefore, the main research questions addressed in this study are as follows: 1) How does the presence of mesoscale turbulent structures affect the water column in our study region? 2) Which mechanisms - reflected by HEV and SPI anomaly signatures - dominate the generation of internal temperature and salinity anomalies within eddies? 3) What is the typical vertical structure of eddies in the Azores Current corridor?

Details of data and analysis methods are described in section 2, and the results obtained are presented in section 3. A brief discussion of the principal aspects of this work is outlined in section 4, and answers to our initial questions are drawn in section 5.



87

88

89

90 91

92

93

94

95

96

97

98

99

100

101

102

103

104

105

106

107

108

109

110

111

112

113

114

115

116

117

118



### 2 Data and methods

#### 2.1 ARGO floats

We used 20997 ARGO individual profiles (https://usgodae.org/cgi-bin/argo\_select.pl) inside our study region between 2000 and 2020. These profiles were later pre-processed considering the following criteria: 1) The profiles' data (temperature, salinity, and pressure) were filtered, retaining those with a GOOD quality flag (equal to 1 or 2 according to https://archimer.ifremer.fr/doc/00187/29825/). Adjusted values were used when available; 2) Profiles with their first value below 20 dbar and the last above 1500 dbar were discarded; 3) each profile should have at least 30 vertical measurements, with a depth difference between two consecutive measurements that should be smaller than 25 dbar from the surface to the 100 dbar level, 50 dbar from the 100 to 300 dbar layer, and smaller than 100 dbar below 300 dbar (these intervals were also used in Chaigneau et al., 2011). In the end, 10034 profiles were retained, corresponding to 48 % of the initial number. The GSW oceanographic toolbox (GSW-OT - www,TEOS-10.org) was used to compute the conservative temperature (CT) and absolute salinity (SA) as well as the mixed layer depth (MLD). All variables were interpolated to 10 dbar levels, and the anomalies of each variable were computed using the World Ocean Atlas 2018 climatology (WOA2018 https://www.ncei.noaa.gov/archive/accession/NCEI-WOA18) for the ARGO period between 2005 and 2017. The climatological data were interpolated in space and time to every ARGO profile latitude/longitude and standard depths. In time, the interpolation consisted of finding the climatological profile for the corresponding year-day, using a 12-month spline interpolation. This method was chosen to reduce bias in temperature and salinity mean fields derived from ARGO floats' contribution to the climatology computation. This bias could be explained by the extended period of data where ARGO floats were not present against the ARGO period, leading to interpolations based on low 3D in situ measurement resolutions.

#### 2.2 Vertical isopycnal decomposition

The vertical isopycnal decomposition (hereinafter ISOD) has been applied not only to investigate the warming and/or freshening of specific water masses (e.g., (Desbruyères et al., 2022) and ocean heat content variability (Zhang and Yan, 2017), but also to examine the vertical structure of mesoscale eddies and the mechanisms responsible for their internal physical and biogeochemical parameters anomalies (e.g. Frenger et al., 2015; Gaube et al., 2014; Keppler et al., 2024). ISOD separates the contributions of two distinct processes to the generation of CT and SA anomalies: eddy trapping, associated with advection along isopycnal surfaces and quantified by SPI, and eddy pumping, associated with the vertical displacement of isopycnal surfaces and quantified by HEV, which is positive (negative) for downward (upward) isopycnal displacements.

In this work, we use the ISOD to characterise the mesoscale structures and infer which process dominates. Following (Bindoff and Mcdougall (1994) and later Han and Yan (2018), the ISOD equation can be written as:

$$\Delta X|p \cong X_{SPI} + (-X_{HEV}) + residue \cong \Delta X|n + (-\Delta p|n\nabla X) + residue$$
 (1)

Where  $\Delta X|p$  represent changes at a pressure level,  $\Delta X|n$  the changes along a given isopycnic surface,  $\Delta p|n$  the difference in pressure for each chosen isopycnal surface reflects the isopycnal vertical displacement ( $-\Delta p|n$  - IVD), and  $\nabla X$  is the



123

124

125

126

128

129

130

131

132

133

134

135

136

137

138

139

140

141

142143

144

145

146

147

148149

150



climatology vertical gradient. A residue (RES) term associated with mixing and/or diffusion, which, for a well-stratified water column, should be near zero. The neutral isopycnal surfaces were used in the evaluation of the terms of HEV and SPI, and were computed using the software available online at http://www.teos-10.org/preteos10 software/neutral density.html

122 (Jackett and Mcdougall, 1997).

The difference between the sum of HEV and SPI and the anomaly for each variable results in the RES term. This term can be associated with double diffusion and/or internal mixing in the eddy's boundaries or its interior, or even other processes (like eddy stirring - e.g. McGillicuddy, 2016) that are not explained by the change of the property along the isopycnics (SPI) or due

to their deflection (HEV); however, their origin is not the scope of this study and will not be referred to.

127 In summary, each ARGO profile was converted into a profile of CT and SA anomalies, as well as IVD, HEV and SPI (for CT

and SA). These metrics will be used to construct the eddy composites, which will then be analysed to show how mesoscale

The mesoscale eddy trajectory atlas product version 3.2 (hereinafter META2022), produced by SSALTO/DUACS and

structures affect the water column in our region.

### 2.3 Eddy tracking and ARGO co-localisation

distributed by AVISO+ (https://www.aviso.altimetry.fr/en/data/products/value-added-products/global-mesoscale-eddytrajectory-product.html), was used to identify and track eddies in ADT maps using a geometric method, and, in this work, only eddies with more than 10 days of tracking were considered. Only tracks with more than 10 days were used. ADT maps between 2000 and 2020 distributed by CMEMS (https://data.marine.copernicus.eu/) were used. ADT was filtered using a first-order high-pass Bessel filter (Mason et al., 2014) with a 700 km wavelength cutoff to remove large-scale variability and then interpolated to every time/location of the ARGO profiles. These maps were used to superimpose the atlas eddy trajectories. In addition to the detected eddies trajectories, the META2022 contains information of their geometry like the speed contour (contour of maximum circum-average geostrophic speed for the detected eddy) or the effective contour (largest contour of the detected eddy) and kinematic properties such as amplitude (A - positive for both cyclones and anticyclones), radius (R) and swirl velocity (U). Additionally, each eddy turbulent energy was computed ( $EKE = \frac{U^2}{2}$ ). One should note that the algorithm used to track the eddies allows the presence of virtual eddies up to a maximum of 4 days, where no speed contours are computed, and therefore these were not used in the ARGO-localisation. The co-localisation of the ARGO floats inside META2022's eddies was conducted, creating a flag for each case where the ARGO float emerged inside the speed contour (i.e., the contour of maximum circum-average geostrophic speed for the detected eddy) polygon that defined an anticyclone - ANT, or a cyclone - CYC. Those that were not inside any speed contour were considered outside an eddy - OUT. A total of 2393 ARGO (31 %) emerged inside eddies and 7641 outside for the AzC system, while for the AzCCo region, a total of 33 % emerged inside eddies, from which 53 profiles are associated with meddies (see Table 1 for more details). The profiles associated with meddies were filtered accordingly to Richardson et al. (1991) and Bashmachnikov et al. (2015) criteria: the CT and SA anomalies should be above 0.5° C and SA anomalies above 0.2 of salinity





for at least 200 dbar between 500 and 1500 dbar. These profiles were later separated from those used in the surface eddies' composites.

Table 1: Number of sampled eddies inside anticyclones (ANT), cyclones (CYC) and outside (OUT) and their number of associated trajectories in the AzC system and in the 3 regions of the AzC corridor.

	ANT	CYC	Number ti	OUT		
	ANI		ANT	CYC		
AzC system	Total	1189	1204	450	439	7641
	R1	244	268	87	85	1625
AzCCo	R2	242	209	91	89	1344
112000	R3	131	116	55	40	649
	Total	617	593	233	214	3618

## 2.4 Composite vertical structure

Although different AzC regions along the current main axis have been identified in previous works (Barbosa Aguiar et al., 2011; Silva-Fernandes and Peliz, 2020), here we emphasise the division associated with the main topographic features and extend our analysis to the western flank of the MAR (Figure 1). Therefore, we will consider three regions: R1 between 20° W and the SWSM chain, R2 from 28° W to the western flank of the ridge following the 2500 m bathymetric, and R3 west of the ridge to 44° W (boxes in Figure 1). To avoid ambiguities in cases of eddies crossing the regions, the eddy is ascribed to a given region depending on the position of the ARGO float and not the eddy itself.

After associating the eddies with different regions, a two-dimensional composite (considering the distance of each ARGO to the eddy centre) and a vertical median profile (of all ARGO profiles inside a region, independently of their position relative to the eddy's centre) of eddy anomalies (CT and SA) and IVD were computed. The latter was used not only to compare the two

the eddy's centre) of eddy anomalies (CT and SA) and IVD were computed. The latter was used not only to compare the two sign structures to the vertical median of ARGO profiles emerging outside eddies along the AzCCo, but also to characterise the vertical structure of meddies as they are found in the eastern part of our domain.

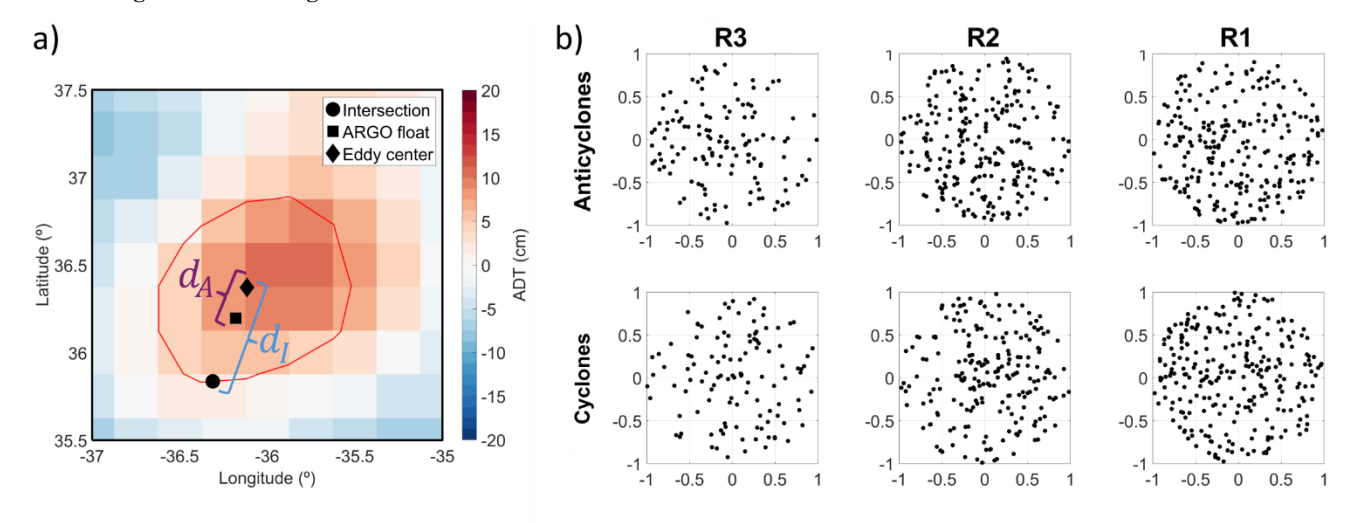
The composites for each region were computed as follows: 1) a normalized distance for each ARGO float to the eddy centre was calculated using the ratio  $(d_A/d_I)$ ; the distance of the ARGO to the eddy centre  $(d_A)$  and the distance of the centre of the eddy centre to the nearest point of the speed contour  $(d_I)$  in the azimuth direction of the ARGO float; i.e., along the line connecting the eddy centre and the ARGO float position (see Figure 2a for more details). Its x (east-west) and y (north-south) components were also computed, being the locations of all ARGO inside the eddies in the regions along the AzCCo represented in Figure 2b. 2) An optimal interpolation (Barnes, 1973) with 3 iterations is conducted to interpolate each variable onto a regular 0.1x0.1 grid at each depth. 3) Further, to build the composites, we have assumed azimuthal asymmetry (i.e., that eddies are circular structures and depend only on depth and distance from the centre). Although this is not verified for all eddies, in





terms of statistics, a first decomposition into zonal and meridional mean sections revealed similar vertical structures (not shown).

Figure 2: a) Illustration of an anticyclone's characteristics: ADT (colours), eddy centre (black diamond), and the eddy speed contour (red line). The float's position (black square) and the intersection of a line (in the direction of the float azimuth) with the eddy speed contour (black circle) are also shown. The distances  $d_A$  and  $d_I$  were used to normalise the distance of every float to the eddy centre. b) Normalised distance of the ARGO profiles to the eddy centre for all points used to construct the eddy composite for the three AzCCo regions and both sign structures



### 3 Results

# 3.1 ARGO distribution and eddy field characterisation

The density of ARGO profiles in boxes of 1x1 degree for ARGO that emerged inside anticyclonic eddies – ANT and cyclonic – CYC are presented in Figures 3a and 3c, respectively.

The higher number profiles for both polarities are located east of the SWSM chain, with the highest values for the cyclonic case (24 profiles). Fewer than 4 profiles are seen in latitudes below 30° N, especially west of 28° W, with some boxes presenting zero ARGO floats emerging inside eddies. ARGO floats emerging outside eddies - OUT (Figure 3e) have their maximum also east of 28° W and in the region centred at 31° N, 39° W. Above the AzP and near the SWSM chain, there are no ARGO profiles located in general due to the shallow topography in that area. In Figures 3b and 3d (for anticyclones and cyclones, respectively), the dynamic characteristics (A, L, U, and EKE) of the META2022 eddies in which the ARGO floats



196

197

198

199

200



emerged can be observed. Despite the cyclones exhibiting a larger dispersion of values for all variables, the median values are similar in both structures, with amplitudes of 5 cm, radius of 80 km, swirl velocities of 20 cm s<sup>-1</sup>, and EKE of 500 cm<sup>2</sup> s<sup>-2</sup>. In

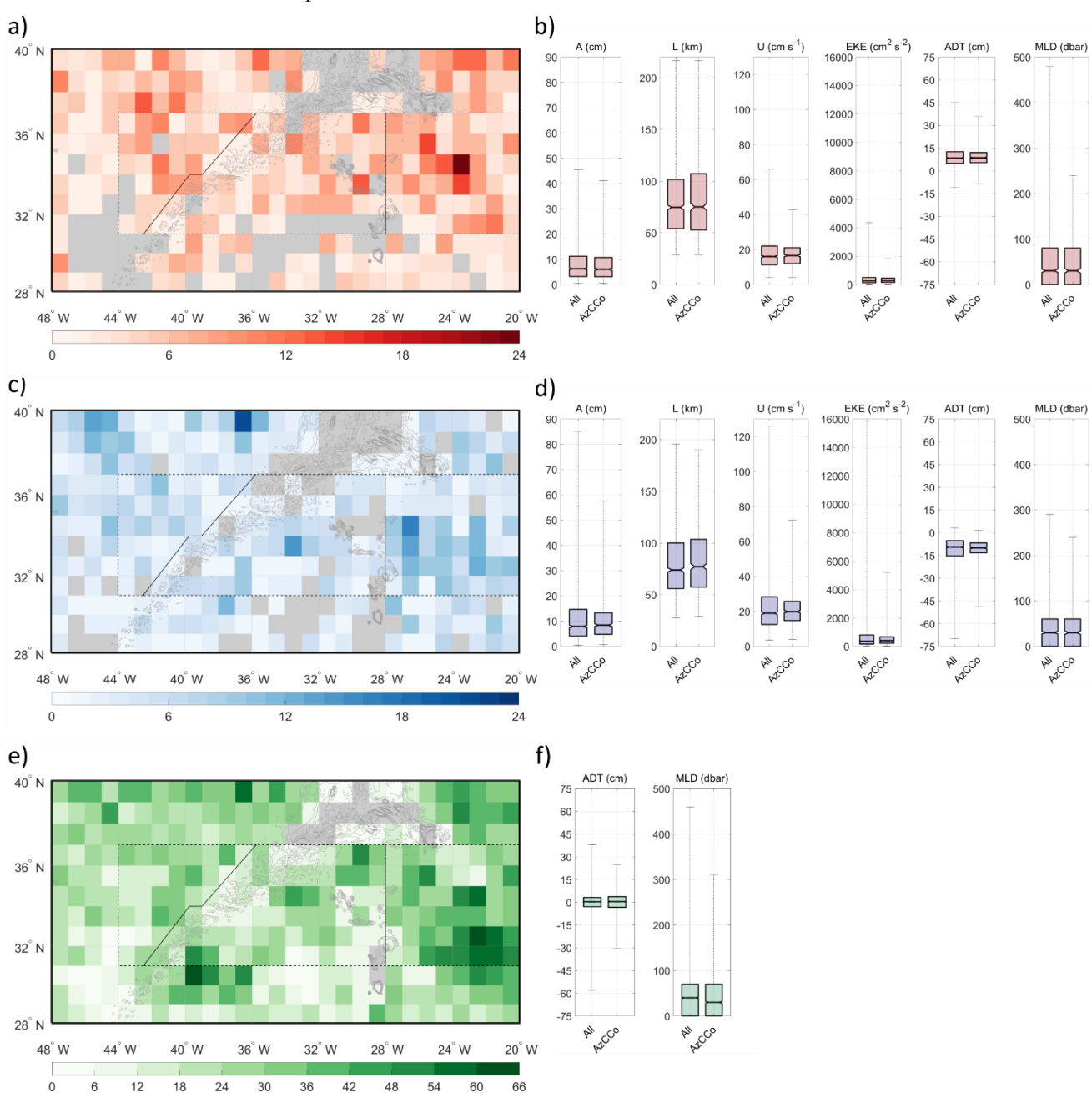


Figure 3: Number of ARGO profiles in boxes of 1x1 degree. Emerged inside anticyclones (a), cyclones(b) and outside eddies (e) and their boxplots of kinematic properties for all region and inside the AzCCo: amplitude (A), radius (R), swirl velocity (U), eddy kinetic energy (EKE); absolute dynamic topography (ADT) and mixed layer depth (MLD) for anticyclones (b), cyclones (d) and ADT and MLD for ARGO profiles emerged outside eddies (f).



201

202

203

204

205

206

207

208

209

210

211

212

213

214

215

216

217

218

219

220

221

222223

224

225

226

227

228

229

230

231

232

233

234



the ADT and the MLD case, they refer to the ARGO location (as for the OUT case - Figure 3f), with the cyclones presenting the larger dispersion of ADT values reaching near -60 cm, but with similar medians between structures, around 5 cm of absolute value, and around zero for the OUT case. The MLD medians are around 50 dbar for the three cases, presenting the anticyclone's higher values reaching near 500 dbar of depth. Regarding the eddies inside the AzCCo they have similar median values with lower dispersion between maximum and minimum, in general, for all variables. One interesting aspect is the higher median value for the cyclones inside the AzCCo when compared to the complete study region. Trajectories of eddies sampled by ARGO floats along their path are presented in Figures 4a and 4b, with a total of 450 anticyclonic trajectories and 439 cyclonic trajectories for the entire study region, and 233 and 214, respectively, for the three regions associated with the AzCCo (Figure 5a, b and c). In the latter, trajectories where meddies were sampled were excluded. The total mean direction of the trajectory is represented in the maps by an arrow located at the point where the beginning of that trajectory detection took place. For the complete study region, there are two areas with lower sampling or even nonexistent in the anticyclonic case: one centred at 31° N - 32° W and the other west of the MAR at 32° N - 44° W. For the cyclonic case, only the region above MAR north of 34° N presents low values of trajectories. Both cyclones and anticyclones present no trajectories above a large region of the AzP. Along the AzCCo, the highest numbers of sampled trajectories are located in the north (south) of the current axis for the anticyclonic (cyclonic) case. Sampled eddies inside our region have most of their origin inside the study area, with most of them also having their end of detection inside (not shown). Their beginning of detection has several different origins (Figures 4a and b), such as the region to the northwest associated with the extension of the Gulf Stream or in the east associated with the Madeira (around 32° N) and the Canary Corridors (around 28° N). A group of eddies (both anticyclones and cyclones) is tracked from the northeast part of our domain to the east of the AzP, having the farthest remote origin of the eddies sampled inside the study domain. Furthermore, observing the total polar graphs in the same figure, it can be observed that the mean trajectory path direction has preferential azimuth directions to the southwest (255°-270° of azimuth) in the case of anticyclones and to the northwest (270°-285° of azimuth) for cyclones. Along the AzCCo (Figures 5a, b and c), it can be observed that most of the sampled eddies' trajectories have their beginning inside (75 %) their respective regions, as well as their endings (78 % - not shown) (see Table 2 for more information). In R1 (Figure 5c), several cyclones have their origin north or west of Madeira Island, while the anticyclones with origin outside R1 come from the northeast of this region. Even though the preferential direction of anticyclones is more random in this region, both sign structures present high relative frequencies to the southwest. Observing R2 (Figure 4b), most of the trajectories of sampled eddies have their origin inside the region or in adjacent regions, with only a few eddies tracked from outside the AzCCo. Also, the cyclones (Figure 5b right) have a clear preferential path to the southwest, but several have directions along the ridge seen above it or in the eastern flank. In the anticyclonic case (Figure 5b left), this region presents preferred path directions to the west with some directions along the ridge also observed above it, as in the cyclonic case. Trajectories of sampled eddies in R3 (Figure 5a) have their origin in the north of this region, with a southwest path direction for most of the

cyclones (seen in the polar graphs). Only three sampled cyclonic eddies (Figure 5a, right) have their beginning of trajectory in





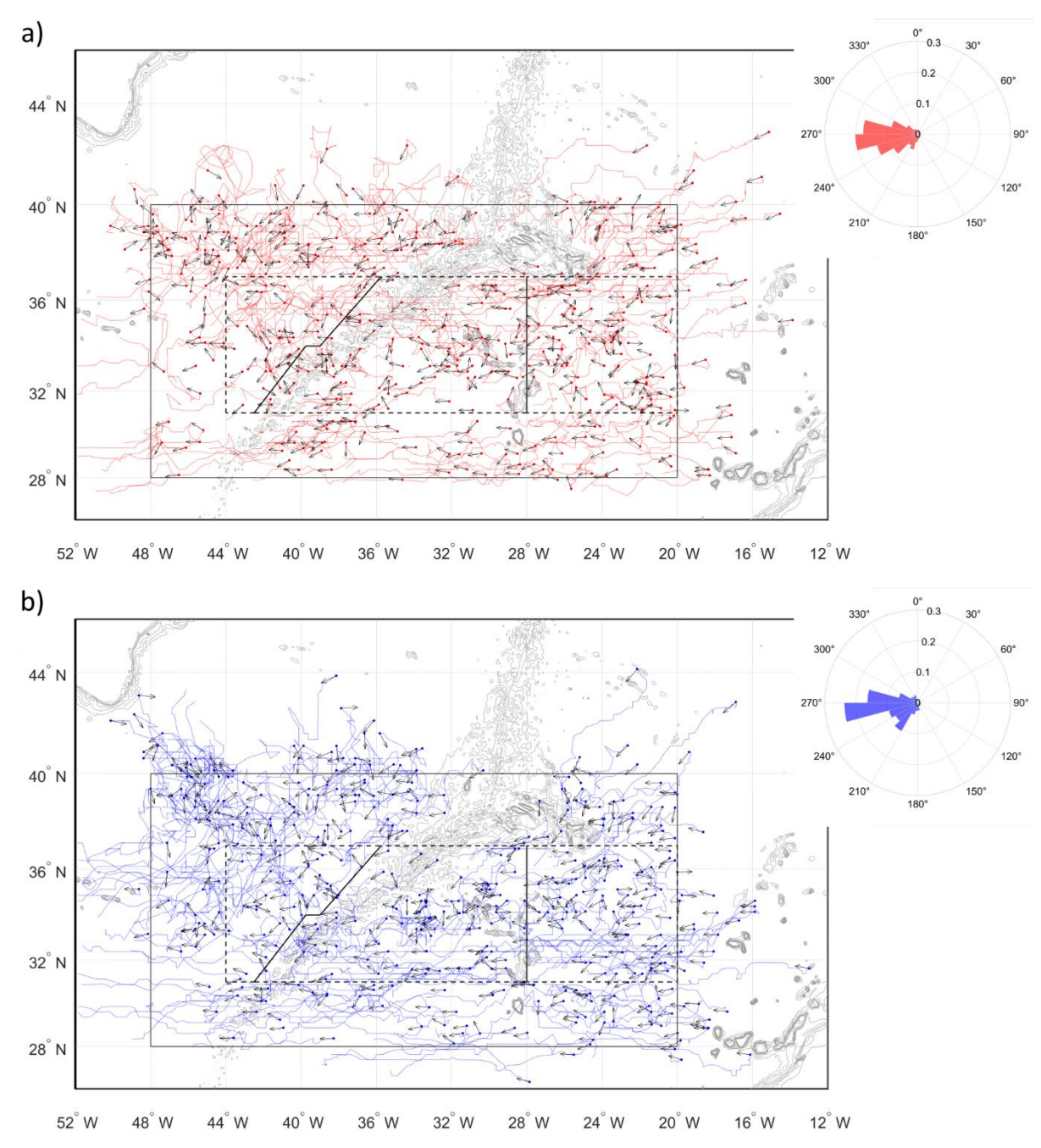


Figure 4: Trajectories (dotted lines) of eddies passing inside the study region (black box) for anticyclones (a) and cyclones (b). Beginnings of detection are represented by points, and the path direction by vectors. The dashed boxes are directly associated with the AzC corridor (AzCCo). The polar graphs represent the relative frequency in each class of the individual trajectory's azimuth, binned in 15-degree classes. The black box represents our study area, and the dashed boxes represent the regions associated with the AzCCo.





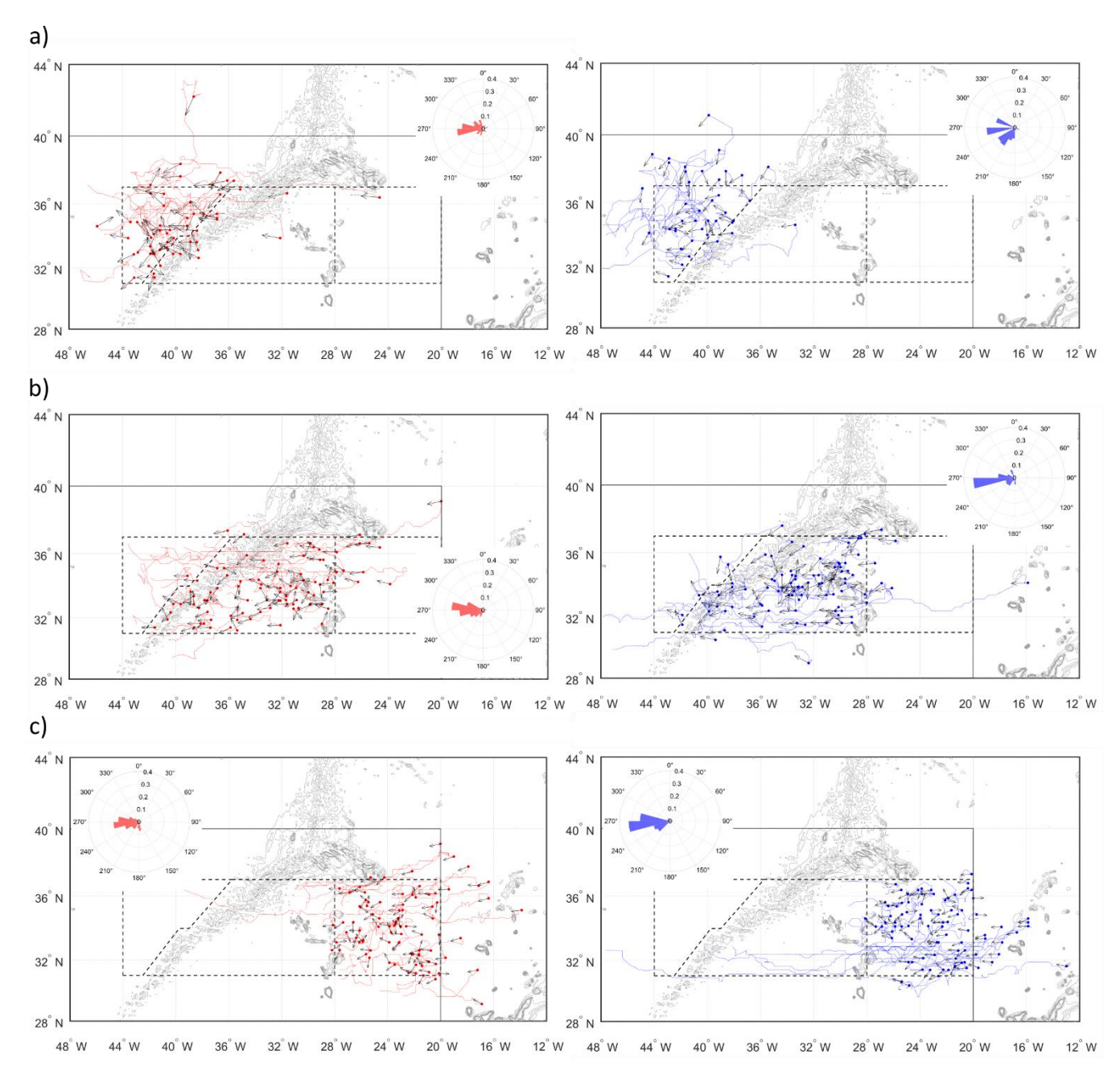


Figure 5: Trajectories (dotted lines) of eddies passing through the AzCCo in region 1 (a), region (b), and region three (c) for anticyclones (left) and cyclones (right). Beginnings of detection are represented by points, and the path direction by vectors. The dashed boxes are directly associated with the AzC corridor (AzCCo). through the AzCCo. The polar graphs represent the relative frequency in each class of the individual trajectory's azimuth, binned in 15-degree classes. The black thin box represents our study area, and the dashed boxes represent the regions associated with the AzCCo.





R2, with two of them already above the ridge, which indicates that the composite of R3 is influenced by eddies with origins west of MAR and is probably related to the Gulf Stream extensions. In the anticyclone case (Figure 5a left), more eddies with origin in R2 are observed, with most of them having their origin above the ridge. Based solely on path trajectories in R3, one could hypothesise that the resulting composite characteristics will be biased towards those of the large eddies associated with the Gulf Stream.

Table 2: Number of individual trajectories of anticyclones (ANT) and cyclones (CYC) that pass inside each region: with their start and end of detection inside each region, on the AzCCo and outside the corridor, respectively.

	ANT CYC		Region			AzCCo				Outside				
		Start		End		Start		End		Start		End		
			ANT	CYC	ANT	CYC	ANT	CYC	ANT	CYC	ANT	CYC	ANT	CYC
R1	87	85	69	66	73	64	2	1	7	13	16	18	7	8
R2	91	89	77	74	71	76	10	9	15	9	4	6	5	4
R3	55	40	29	20	38	27	17	5	7	1	9	15	10	12
Total	233	214	175	160	182	167	29	15	29	23	29	39	22	24

#### 3.2 Mean zonal and meridional structure

The climatological meridional (Figure 6a) and zonal (Figure 6b) vertical means for the ARGO period in the three regions along the AzCCo are shown in Figure CT (left) and SA (right).

A clear deepening from north to south is observed in both the isotherms (Figure 6a left) and isohalines (Figure 6a right) of the meridional means in R1 and R2 linked to the presence of the Azores Front located around 34° N, characterised by colder and fresher waters in the north and warmer and saltier waters to the south. Its signature spans to depths of around 750 dbar in the CT mean (Figure 6a left), appearing to be shallower for the mean. In R3, the same pattern is observed but less pronounced than in the east of MAR. Furthermore, at 1500 dbar, the intrusion of colder waters (CT below 5° C) occurs in this region, resulting in a higher gradient of temperatures in the water column. The same is observed on the meridional mean, where the temperature gradients grow from east to west (Figure 6b left).

The penetration of the MW from the east can be observed in the SA meridional mean R1 (Figure 6a right), noticeable by the intrusion of waters with higher salinities below 1000 dbar at 20° W. In R2, a water mass with a distinct pattern is observed at the same depths, being linked with the propagation of the MW to the west, as also seen in the zonal SA mean (Figure 6b right). A peculiar aspect of this mean field in R1 (Figure 6b right) is its homogeneity spanning from 750dbar depth to 1000 dbar depth. In R3 at 1500 dbar, the upwelling of fresher waters (SA below 35.3) is observed both in the meridional and zonal means, which, in association with the lower temperatures seen in the CT means, show us that the two basins (east and west of MAR) have distinct characteristics at depth (1500 dbar).





274

275

276

277

278

279

280

281

One should note that due to the way regions 2 and 3 boxes were constructed, the meridional mean in R2 (R3) west (east) of 40° W will reflect more the south (north) part of the AzCCo, and in the east (west) the northern (southern) part.

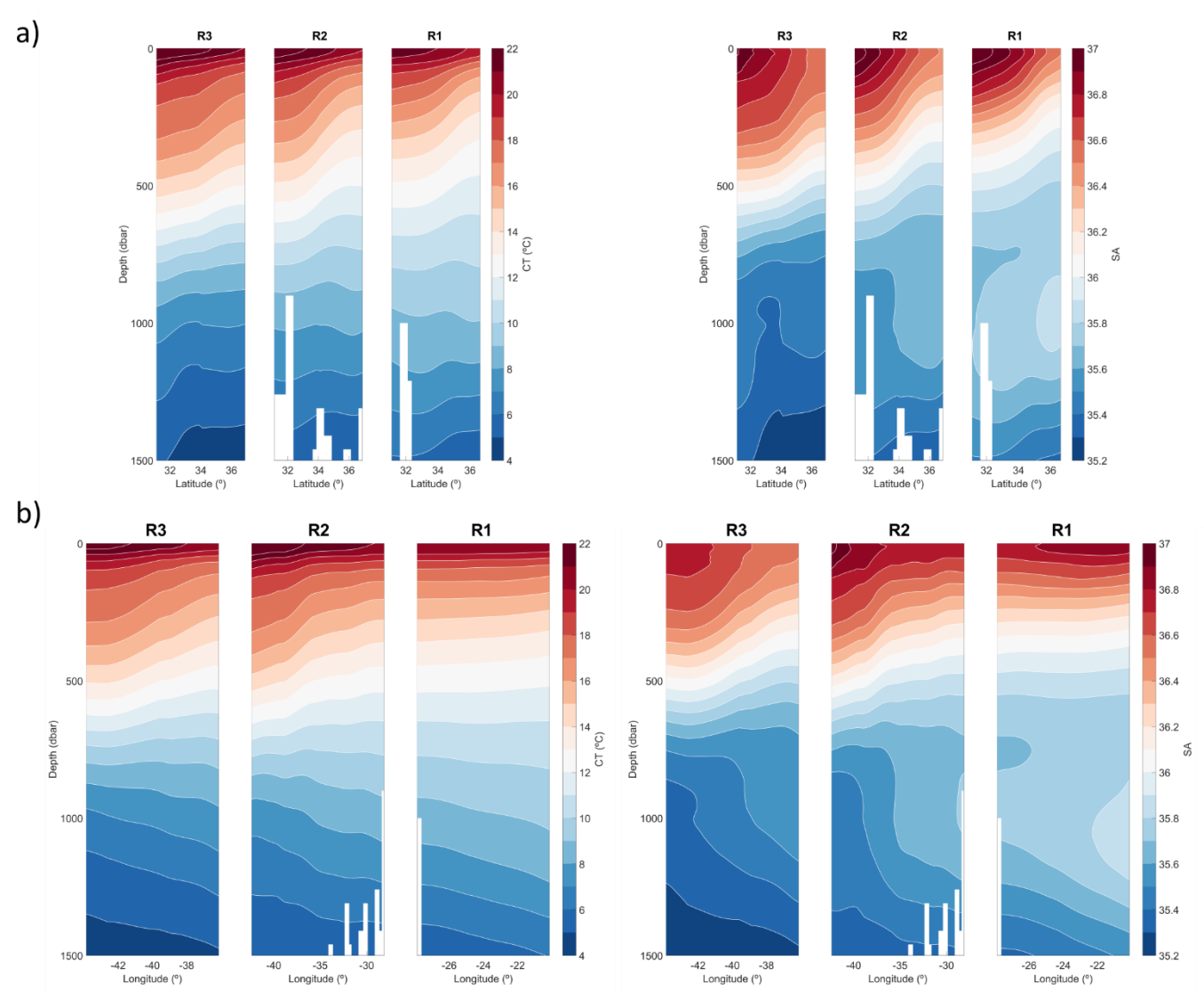


Figure 6: Meridional (left) and zonal (right) CT climatology mean inside the three regions associated with the AzCCo. (b) The same as (a) but for SA climatology. White pixels represent the topography of the region associated with the SWSM chain and the shallower part of MAR.

# 3.3 CT/SA vertical structure

The CT and SA composites for both sign structures along the AzCCo are presented in Figure 7. The sampled eddies that present meddies' characteristics at depth were separated from the others to obtain a better representative composite of the





surface eddies in this region, since they are the main object of this study. Nevertheless, the vertical median structure of meddies (sampled in anticyclones and cyclones) is presented in Sect. 3.5. The asymmetrical internal structure between anticyclones and cyclones is observed both in CT and SA vertical composites across the three regions. A deflection of isotherms (Figure 7a) and isohalines (Figure 7b) downward (upward) from the centre of the composite to its boundary in the anticyclonic (cyclonic) case is visible, being more intense in the isohalines case.

From east to west, there is an intensification of the CT vertical gradient between the east (R1 and R2) and the west (R3) of the ridge, where colder waters can be observed at the 1500 dbar level, reaching values below 5° C. This upwelling of colder waters is seen in both anticyclones and cyclones in R3, even though they are also present in R2 cyclones at the 1500 dbar level.

The SA composite vertical structure is highly asymmetrical between the two basins (east and west of MAR). The SA vertical structure in R1 presents a layer of constant SA (between 35.8 and 35.7 of salinity) with ~750 dbar of thickness in both sign structures, being located deeper (shallower) in the water column in the anticyclonic (cyclonic) case. This layer is also observed in R2, having less vertical spanning. R3 presents both lower values of SA at the surface as well as the intrusion of fresher waters (salinity below 35.2) at the 1500 dbar level when compared to the eastern side of the MAR. The deflection of isohalines is more pronounced in R3 with downwelling (upwelling) of the isohalines of about 75 dbar from the centre to the boundary in the anticyclonic (cyclonic) case.

# 3.4 The isopycnal decomposition

The ISOD along the AzCCo is analysed in this section for both the anticyclonic and cyclonic 2D composites. Figures 8 show the radial composite of the anomalies, HEV, SPI, and RES for both variables, CT and SA, as well as the IVD.

A significant asymmetry between anticyclones and cyclones is observed in both CT (Figure 8a) and SA (Figure 8b) anomalies for the three regions, both in terms of vertical structure, magnitude, and sign. While cyclones present a well-defined core, anticyclones present a more vertically elongated structure, especially in R2 throughout the water column. A deepening of eddies' core is also observed with depths of 250 dbar for cyclones in R1 to 500 in R3, and from 250 dbar to 750 dbar for anticyclones. An inversion of the shallowest core between the sign structures from east to west is observed. Anticyclones' core is warmer and saltier, reaching more than 0.75° C and 0.1 of salinity in all regions, while cyclones have a colder, fresher core with the highest values of anomalies below -2° C and -0.3 of salinity in R3 (Figure 8b left). In R1 for both structures and R2 for cyclones, a minimum in the CT anomaly (Figure 7a, right and centre) is observed around 1000 dbar. Around the same level and for a deeper vertical extension, an inversion in the SA anomaly (Figure 8b, right and centre) sign is present, associated with the downwelling (upwelling) of the MW in the anticyclonic (cyclonic) case due to the deflection (elevation) of the isopycnics at those levels. In R2, the vertical structure of CT for the anticyclone composite appears as if it retains characteristics of both R1 and R3, as it presents an elongated core from surface to the 1000 dbar level with a maximum at 750 dbar. This can be the result of the anticyclone sampling in this region being made above the ridge in R2 near the border with R3.



316

317

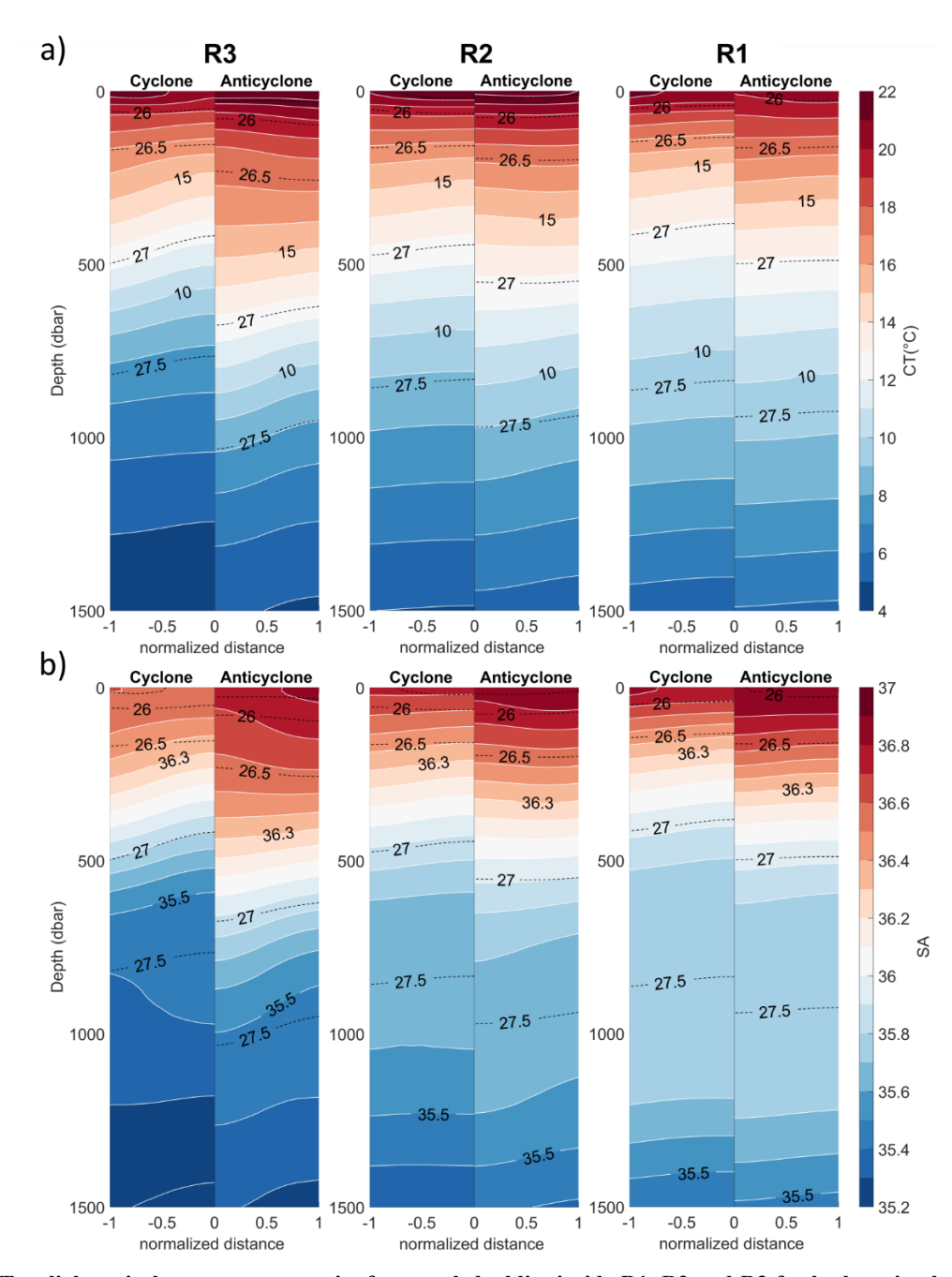


Figure 7: (a) CT radial vertical structure composite for sampled eddies inside R1, R2 and R3 for both anticyclonic and cyclonic structures. Dashed lines represent the density anomaly (kg m<sup>-3</sup>) relative to the surface. (b) The same as (a) but for the SA radial vertical structure composite.





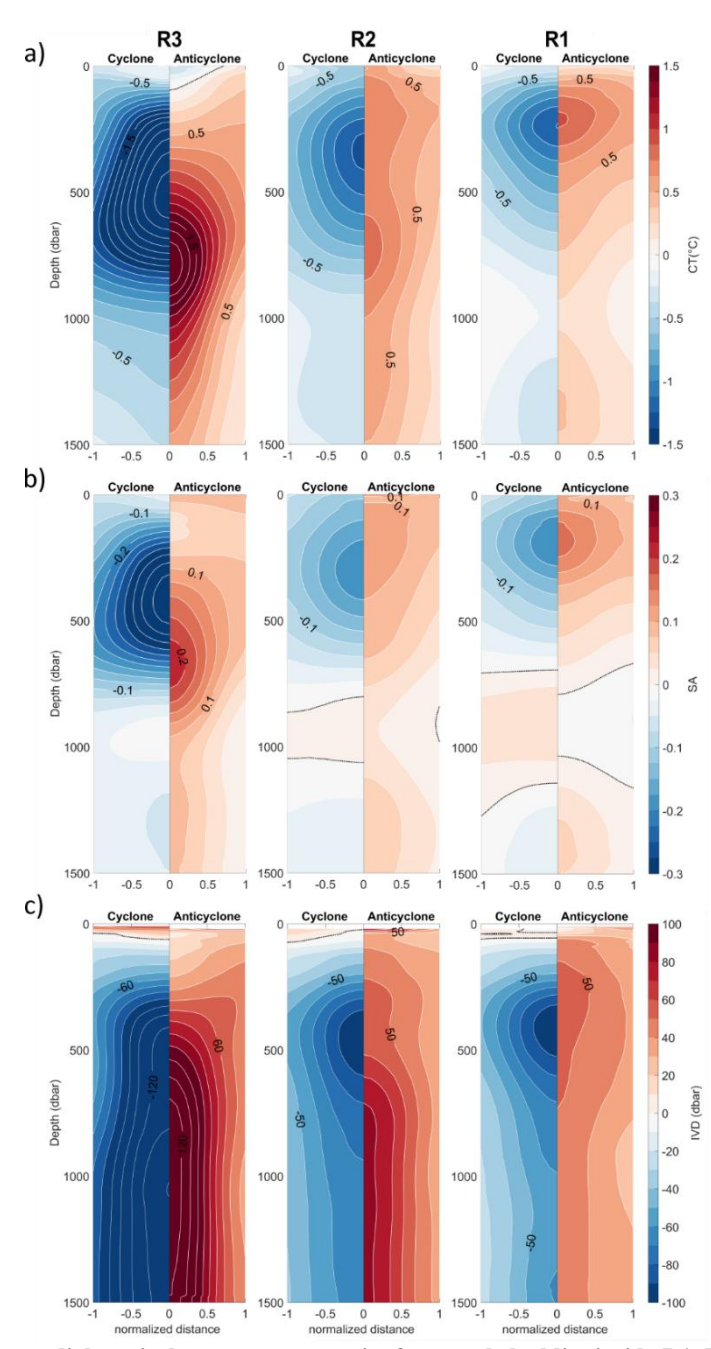


Figure 8: ISOD decomposition: radial vertical structure composite for sampled eddies inside R1, R2 and R3 for both anticyclonic and cyclonic structures. (a) CT anomaly, (b) SA anomaly, (c) Isopycnal Vertical Displacement (IVD). The dotted black line contour represents zero for that variable.



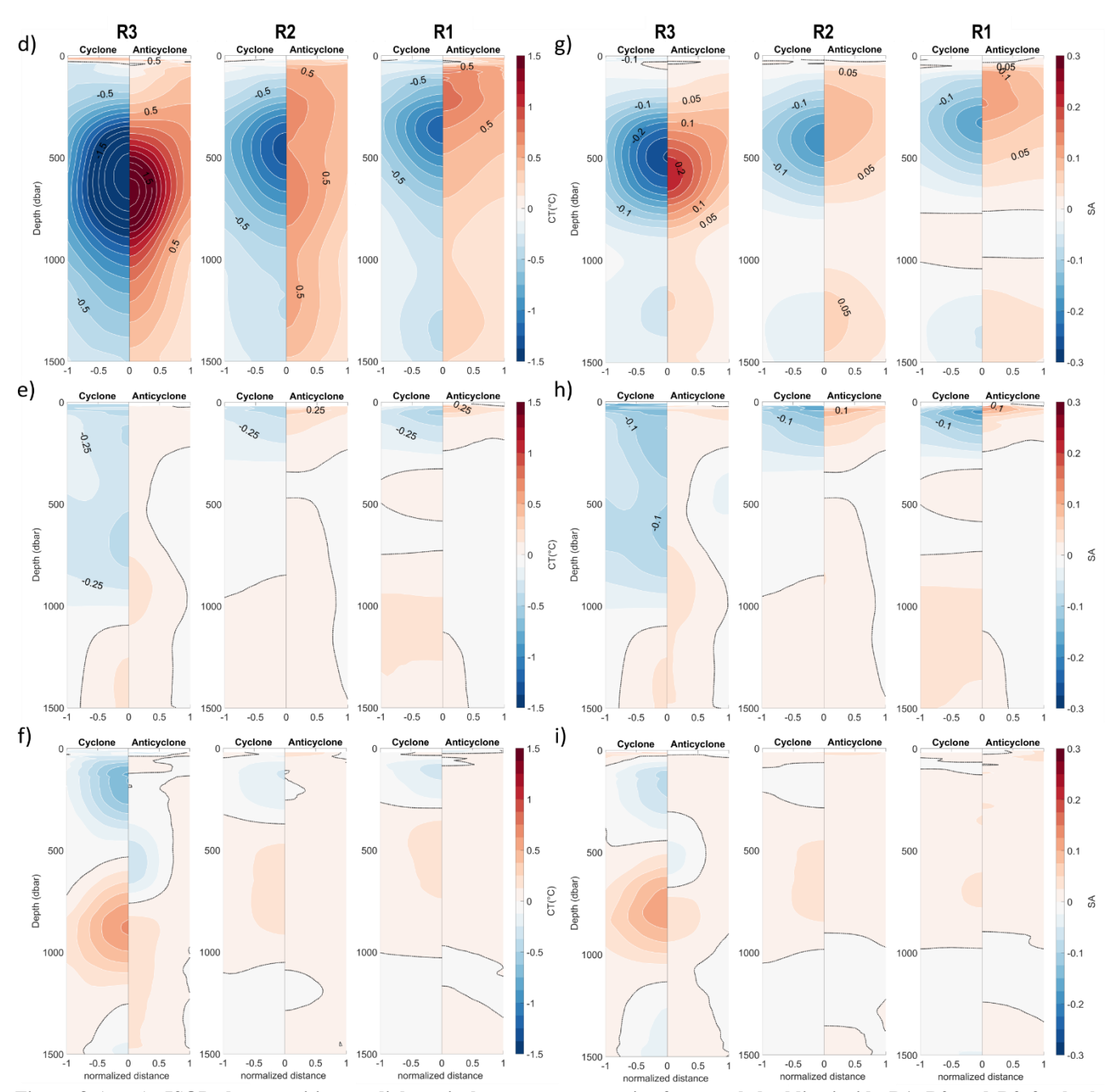


Figure 8 (cont.): ISOD decomposition: radial vertical structure composite for sampled eddies inside R1, R2 and R3 for both anticyclonic and cyclonic structures. (d) CT HEV, (e) CT SPI, (f) CT RES, (g) SA HEV, (h) SA SPI, (i) SA RES. The dotted black line contour represents zero for that variable.

328

325

326



329

330

331

332

333

334

335

336

337

338

339

340

341

342

343344

345

346

347

348

349

350

351

352

353

354

355

356

357

358

359

360

361

362



The vertical displacement of the isopycnics surfaces inside the eddy structure is confirmed by the IVD (Figure 8c) sign. As observed in Figures 8c, right and centre, the anticyclones (cyclones) present positive (negative) signs reflecting the deflection (elevation) of the isopycnics. Also in this case, there is a clear asymmetry between sign structures, being well-defined in the cyclonic case and presenting higher values (below -90 dbar in R1 and R2 and -130 dbar in R3). In the cyclonic case, the IVD structure is very similar in the east of MAR, with only a slight deepening of the maximum from R1 to R2, while in R3, the cyclonic core presents a more barotropic structure, with constant values at increasing distances from the centre from 400 dbar depth to 1500 dbar. The same barotropic structure is observed in anticyclones on both sides of the ridge, being more pronounced in R2 and R3, reaching values above 80 dbar and 120 dbar in R3 at a depth around 750 dbar. For all regions, the IVD at 1500 dbar is non-zero, presenting values above 40 dbar for both cyclones and anticyclones, which indicates that the eddies' influence on the water column is deeper than that depth. HEV (Figures 8d and 8g) present values clearly higher than those for SPI (Figures 8e and 8h) for both variables and both structures, being indicative that the vertical movement of the isopycnic surfaces has a higher impact on the anomalies' formation inside the eddies' core. The maxima of HEV are located at a slightly deeper level than those of the anomalies, with the same deepening to the west. It presents a range of values from lower than -1° C to -1.5° C in the west for cyclones and between higher than 0.5° C to 1.5° C for anticyclones. This component is always positive for anticyclones and negative for cyclones in the CT case (Figure 8d), indicating that the signature of the eddies in the density field is uniform in the upper 1500 dbar. As for the IVD, HEV is also non-zero at depth, supporting the hypothesis that anticyclones and cyclones have a deeper structure than 1500 dbar. One aspect of the SA HEV (Figure 8g) in R1 is its sign inversion below 750 dbar associated with the MW top boundary, resulting in an inversion (not shown) in the climatology gradient ( $\nabla pX$  - see equation 1) sign at those levels. From east to west, the maximums range between -0.15 for cyclones to lower than -0.2 in the cyclonic case, and from 0.075 to more than 0.125 of salinity. Both CT and SA HEV present higher values in the cyclonic case for the three regions, being the same observed in the IVD case. The SPI structure (for both structures and variables) is more complex than that of HEV. In the east, the CT SPI (Figure 8e), higher values (lower than -0.25° C and higher than 0.125° C) are mostly confined to the upper layers, i.e., in the first 250 dbar with generally higher values than HEV at those pressure levels, especially in the anticyclonic case, with a sign inversion below that level with a higher vertical extension in R1. West of MAR, anticyclones present the same sign throughout the water column for anticyclones and to the 1000 dbar level for cyclones. A similar vertical structure is observed in the SA SPI (Figure 8h) for both structures and all regions, respectively, reaching values lower than -0.1 in the cyclonic case and higher than 0.025 for anticyclones. The maxima in the eddy core are located shallower in the water column compared with the anomalies' maximum depths. Although the analysis of the ISOD's residues is not an objective of this work, it can be observed (Figures 8f and 8i) that for both fields the RES vertical structures present values of the same order as the SPI component, indicating that the process of

diffusivity and/or diapycnal mixing or even other processes (like eddy stirring) that are not explained by HEV or SPI





contributes with the same magnitude as the SPI component for both the CT and SA anomalies. In the CT RES case (Figure 8f), for all regions, a well-defined structure for cyclones is observed, located at the same depths as the anomaly's cores, indicating that these processes could be a key component to define the cyclones' internal vertical structure. The same is observed in the SA RES (Figure 8i) in R3.

3.5 Median vertical structure

The 10-day mean direction of the sampled eddies along the AzCCo is presented in Figures 9 for both anticyclones (Figure 9a) and cyclones (Figure 9b). Some preferred directional paths emerge for both structures. Observing the polar graphs, most of R1's sampled cyclonic eddies have azimuths approximately to the west (between 255° and 285°), with anticyclones presenting a more dispersed path direction. In R2, while anticyclones present a preferred path to the west with several eddies with clear westward trajectories, cyclones present a more random path direction with higher relative frequencies to the west and southwest. An interesting aspect of the direction of these sampled eddies in R3 is that many of them present a mean direction to the southwest in both anticyclones and cyclones (higher in the cyclonic case), indicating that the eddies' trajectory has a north origin instead of an eastern one.

To compare the vertical structure of eddies in the AzC System with the CT and SA anomalies for the background, medians of all profiles inside each region were computed and compared to the median of the profiles emerging outside eddies (OUT profiles) for that region. Furthermore, these vertical profiles were used to better describe differences between the regions for the AzCCo. In Figure 9c, the medians of CT and SA anomalies and IVD are presented for both anticyclones (thick red) and cyclones (thick blue), as well as their 10th and 90th percentiles (thin lines) for the three regions. The thick black line represents the median of the OUT profiles.

The OUT median for both CT and SA anomalies is zero along the AzCCo in the water column, even though their percentiles still present significant values (the shaded area of the percentiles is not shown in the figure). This could indicate processes associated with meanders and/or filaments that are not captured by the eddy detection algorithm; virtual eddies (see Sect. 2.4); or even being associated with other processes like Rossby waves.

There is a clear asymmetry between anticyclones and cyclones along the corridor and for the 3 variables. The CT anomaly medians are always positive (negative) for anticyclones (cyclones) throughout the water column. The maxima are more defined in the cyclones case, with a deepening in the water column from east to west, from 250 dbar to 600 dbar, and are also more intense west of the ridge. For anticyclones, their maximum varies from 250 dbar to 750 dbar in the west, increasing also in intensity. In R2, one can observe that the CT anomaly vertical profile is more barotropic than the 2 other two regions, with a constant value from the surface to 1500 dbar.

From east to west, there is a deepening of the SA anomaly median's zero from above 750 dbar in R1 to below that level in R2 and just above 1000 dbar in R3 for both sign structures. Being associated with the MW presence, its zero is visible across the AzCCo and is followed by an inversion of the SA anomaly's vertical sign (from negative to positive) in R1 in the cyclonic





case, where the presence of the MW is more pronounced. In the anticyclonic case, a slightly negative anomaly is observed at the same depth, resulting in the downwelling of the MW upper boundary by the anticyclone internal deflection of the isopycnics. The same vertical pattern towards zero is exhibited by the CT anomaly in R1, but without the inversion of its median.

The IVD median's vertical structure is almost homogeneous for the anticyclones from the surface to the 1500 dbar, indicating that their internal structure is more barotropic than that of the cyclones, which in R1 and R2 present a maximum above the 500 dbar level. The IVD sign is always positive (negative) in the anticyclonic (cyclonic) case in all regions, which indicates that the eddies' presence influences the water column to the 1500 dbar. Furthermore, as the values of median IVD at this depth are still significant as well as their 90th percentiles (~ 100 dbar in R1 and R2 and ~200 dbar in R3), this means that these structures have an influence that can reach depths below the 1500 dbar level.

As meddies are well-known structures present in our study region, their vertical structure is also analysed in this section. Even though they are not the main object of this work, their structure being well-known helped us to better understand the SPI and HEV concepts and their relation to the eddies' internal vertical structure. The search for sampled meddies profiles was not restricted to those inside the AzCCo but extended it to the east of the AzP, as they are also commonly tracked in that area. The 10-day mean direction of the sampled meddies is presented in Figure 9a, and their median CT, SA, and IVD vertical structure in Figure 9b.

The sampled meddies south of 38° N usually present with some exceptions, western directions, while those north of that latitude exhibit southwest directions. These meddies are grouped according to their sign at the surface, as the ARGO float emerged inside a surface cyclone or anticyclone. A major difference emerges from their vertical structures: while cyclones are colder and fresher until the 600 dbar depth, the ones sampled inside anticyclones show a slightly warmer and saltier structure until that depth. Below that level, all present warmer and saltier structures to the 1500 dbar depth, with the anticyclones presenting higher anomalies reaching values of 4° C and 0.8 of salinity against 1° C and 0.25 of salinity. Furthermore, the depth of the median maximum is shallower in the anticyclonic case, with the cyclonic median being more constant at depth. Another difference that can be observed is the asymmetrical structure of the IVD; anticyclones show clearly high positive values, while cyclones have mainly negative ones. This could indicate that we are both in the presence of anticyclonic meddies (positive IVD) and cyclonic meddies (negative IDV). The sampling of meddies by these profiles is corroborated by the CT-SA diagrams (not shown), where higher values of CT and SA are observed, conforming with those associated with meddies. Furthermore, the 10th percentile of the cyclones' IVD presents a sign change at around 1000 dbar, which could indicate that some of these profiles sampled anticyclonic meddies.



431

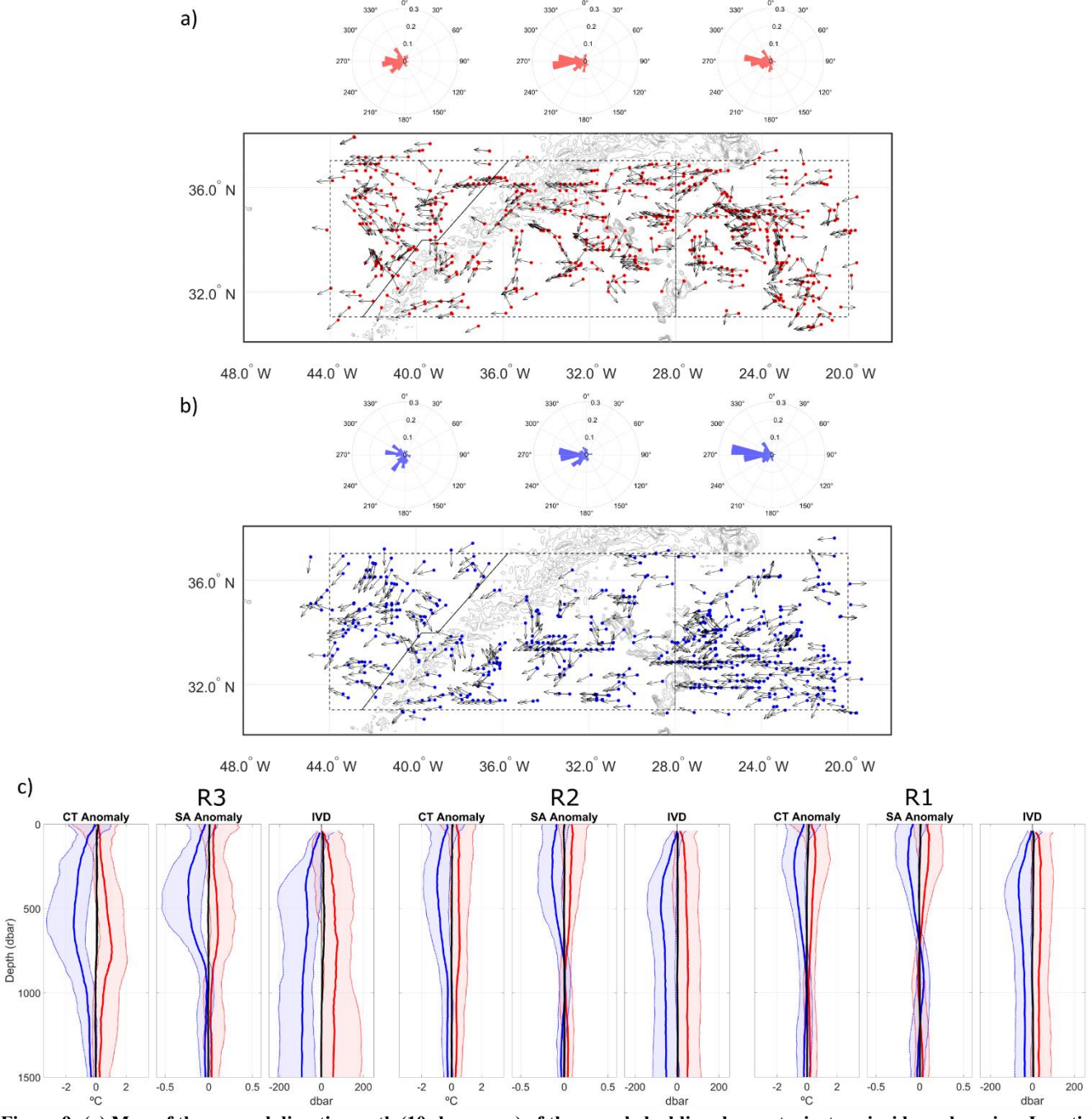


Figure 9: (a) Map of the general direction path (10-day mean) of the sampled eddies along a trajectory inside each region. Location of the sampled eddies represented by points and the path direction by vectors. The polar graphs represent the relative frequency in each class of the individual trajectory's azimuth, binned in 15-degree classes. (b) Median vertical structure of the eddy composite for both sign structures (anticyclone red and cyclone blue) and the median vertical structure of the outside eddies (black) for the three regions associated with the AzCCo: R1 (right), R2 (centre), and R3 (left) for the CT and SA anomalies and the vertical displacement, IVD.





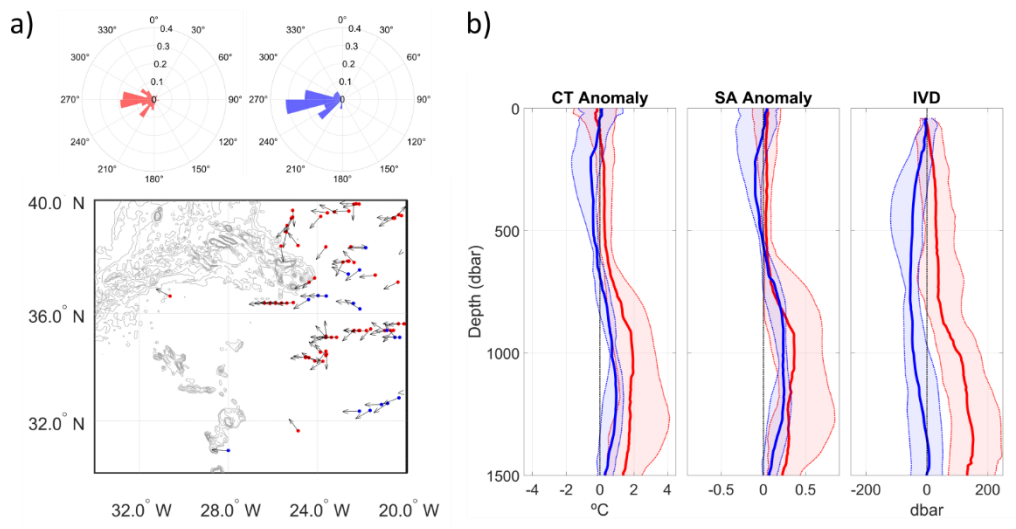


Figure 10: (a) Map of the general trajectories of the sampled meddies (anticyclones red and cyclones blue) for a period of 10 days. The polar graph represents the relative frequency in each class of the individual trajectory's azimuth, binned in 15-degree classes. (b) Median vertical structure of the meddies' profiles for both sign structures (anticyclone red and cyclone blue) for the CT and SA anomalies and the vertical displacement, IVD.

### 4 Discussion

### 4.1 West-east eddies' origins

Zonal differences in the eddy's vertical structure along the current main axis are more pronounced between the east (R1 and R2) and west of MAR (R3), as the ridge acts as a boundary for two areas with very distinct dynamics. From east to west, a deepening of the anomaly's maxima, accompanied by increased intensity (from absolute values above of 0.5° C and 0.1 of salinity to more than 1.5° C and 0.2 in salinity in the west) and the vertical extension in the water column (from 750 dbar to 1250 dbar in the west), is observed both in the 2D radial composites and in the median vertical structure for both CT and SA. Along the AzCCo, anticyclonic eddies present warmer, saltier cores, while cyclones have cold, fresh cores with a clear, more baroclinic structure.

The diverse origins of the sampled eddy trajectories used in the AzCCo composites construction can be attributed to the observed differences. East of the MAR, the R1 eddy composite is predominantly constructed using profiles of eddies with origin inside that region, with some having their beginning of detection in the northeast of the AzP in the anticyclonic case and north of Madeira Island for both anticyclones and cyclones. In the latter case, these eddies may have two possible origins: either from the evolution of AzC meanders, leading to the formation of eddies that propagate westward, or from the interaction of those with eddies originating in the Canary Upwelling System, which can propagate westward to longitudes as far as 40°W, as previously reported by Pegliasco et al. (2015) and Sangrà et al. (2009). In R3, the sampled eddies' trajectories' azimuths demonstrate directions from the north and east, primarily in the cyclonic case. Furthermore, a migration of eddies to the south



455

456

457

458

459

460

461

462

463

464

465

466

467

468

469

470

471

480

481

482

484

485

486

487



on the western flank of the ridge is observed both on the global azimuths of the R3 trajectories and the sampled eddies' trajectories' azimuths. Ollitrault and Colin de Verdière (2002) reported, based on the trajectories of SOFAR floats launched on each side of the ridge, that eddies are frequently found to travel southward along the western ridge's flank. However, they also found that, after the floats span the western basin between 30° N and 45° N, eddies are also found to travel towards the ridge. Furthermore, Caldeira and Reis (2017), using eddy trajectories tracked on altimetry data (Chelton et al., 2011) and the computation of the zonal and meridional Ekman transport, reported that the Azores Archipelago (in this work represented in the northwest, centre, and southeast of the AzP) is a confluence zone of far-field eddies with different origins. The northwestern and central regions are predominantly influenced by the Gulf Stream, filaments, meanders, and eddies, while the southeastern region is impacted by eddies that are likely to have originated from the meandering AzC pinching. This is consistent with the hypothesis that eddies in R3 are primarily a byproduct of the merging and splitting of mesoscale structures with different origins: those generated in the east and crossing the ridge, and those generated by the evolution of the Gulf Stream branches, migrating to the south along the western flank of the ridge. R2 is a transitional region encompassing the MAR, with eddies originating on both sides of the ridge and above it. The composite vertical structure of eddies in this region exhibits characteristics of both R1 and R3, presenting an elongated core that spans nearly the entire water column. This structure reflects the shallower cores of R1 as well as the deeper cores of R3, influenced by the presence of eddies that may originate from the Gulf Stream system, evident in both CT and SA anomalies.

#### 4.2 HEV vs SPI

472 HEV is clearly the predominant contributor to the vertical structure of both CT and SA anomalies on both sides of the MAR 473 throughout the water column, with SPI exhibiting higher values in the first 250 dbar east of MAR and a larger vertical extension 474 on the west. Along the AzCCo in R1 and R2, HEV presents well-defined maxima for anticyclonic (cyclonic) structures around 475 the 400 dbar (500 dbar) level, indicating that these structures' anomalies are mainly generated by the depression (elevation) of 476 the isopycnic surfaces, resulting in the downwelling (upwelling) of warmer (colder) waters and consequent warm (cold) 477 anomalies. West of MAR, the same dominance in depth of HEV and SPI is observed, reaching higher values and vertical 478 spanning with the same vertical extension observed for the IVD.

479

Low SPI values in our region, despite their dominance at the surface, can be explained by the fact that most eddies sampled in the composites originate and dissipate within the AzCCo. As these eddies travel westward, the CT and SA fields are nearly zonal, so the advected waters retain properties similar to the background climatology, resulting in only minor variations along isopycnal surfaces. In contrast, for meddies (not shown), which advect MW with properties highly contrasting the background, SPI values at depth exceed those of HEV, reaching values above 2°C and 0.5 in salinity.

483

Four mechanisms have been identified as contributing to the transport of physical and biogeochemical properties by eddies: eddy pumping, eddy trapping, eddy-induced Ekman pumping, and eddy stirring. He et al. (2024), using altimetry combined with extensive in situ hydrographic measurements from the World Ocean Database, demonstrated that, at a global scale, temperature anomalies within eddies are primarily impacted by eddy pumping. This is in accordance with the low values of





relevant, which is the case of the MW by meddies in our region. Frenger et al. (2015) show that the sign of the anomaly resulting from eddy trapping is determined by the horizontal temperature gradient in the direction of the eddy movement, which, in our case, is generally to the west. This study also supports our hypothesis that low SPI values are indeed associated with a meridional gradient of temperature and salinity in the first layer east of the ridge. Contrarily, the high values of SPI observed (not shown) in the meddies case are a result of the sharp zonal gradient of both temperature and salinity at depth, east of the ridge, due to the penetration of the MW to the west.

Several regional studies (e.g., Keppler et al., 2018; He et al., 2023) have shown that eddy-induced anomalies near the surface primarily originate from eddy trapping, whereas at greater depths, eddy pumping is the dominant mechanism. Moreover, Amores et al, (2017), concluded that the mean temperature and salinity anomaly profiles in their northern region (which covers part of our study region, south of the current axis and east of the ridge) are dominated by advection in the first 200 m and the vertical displacement of mean isopycnal surfaces below 300 m. The authors also report an eddy signal as deep as 1200 m, which is consistent with the fact that the HEV values do not converge to zero at the 1500 dbar and the high values of IVD across all the AzCCo east of the ridge. These findings suggest the potential for these mesoscale structures to exert a deeper influence on the water column. As previously documented by Pingree et al. (1996) and Mourino et al. (2003) analogous deep signals of eddies have been reported in the range of 100 dbar to 1500 dbar and 200 m to 4000 m depth, respectively.

SPI found in our region. In regions with large horizontal temperature gradients, He et al. (2024) claim the eddy trapping to be

#### **5 Conclusions**

In this study, we analysed the CT and SA profiles of ARGO floats emerging within tracked eddies (both anticyclones and cyclones) on ADT maps. The main objective was to characterise the vertical structure of mesoscale turbulence in our study region (along the AzCCo) and understand its impact on the water column. Our findings can be summarised as follows.

The vertical structure differences found between the east and the west side of the ridge are associated to different origins of the sampled eddies: while in the in the east, they have mainly their origins inside their respective region, in the west, the majority have origins outside R3 being a combination of eddies travelling from the east and from the northwest, this latter associated to Gulf Stream eddies, resulting in more intense anomalies of the composites.

Regarding the influence of the mesoscale turbulence in the water column, this work showed that: 1) From east to west, the absolute maximum value of both CT and SA anomalies is found at higher depths, from 250 dbar to 750 dbar. 2) Anticyclones (cyclones) present a more barotropic (baroclinic) structure. 3) IVD absolute values exceeding 50 dbar from the surface down to 1500 dbar confirm the deep-reaching influence of both anticyclonic and cyclonic eddies on the water column. The high IVD absolute values (above 150 dbar) across the AzCCo further indicate that these structures could have the potential to enhance vertical advection, not only of heat and salt but also of biogeochemical properties.

When exploring the HEV and SPI signature and intensity, we concluded that: 1) The HEV component is the main contributor to the formation of the CT and SA anomalies, as it exhibits the highest values along the AzCCo. 2) This dominance indicates

https://doi.org/10.5194/egusphere-2025-5507 Preprint. Discussion started: 19 November 2025

© Author(s) 2025. CC BY 4.0 License.



520



521 anomalies due to the downwelling (upwelling) of the shallower (deeper) isopycnal surfaces in the anticyclonic (cyclonic) eddy 522 interior. 3) SPI shows lower values across the domain, with higher values in the first 250 dbar east of the MAR when compared 523 to HEV, reflecting the eddy surface tendency to trap different water masses. 524 Data availability 525 This study has been conducted using E.U. Copernicus Marine Service Information altimetric 526 https://doi.org/10.48670/moi-00148. The ARGO float data were extracted from https://usgodae.org/cgi-bin/argo\_select.pl, and 527 the temperature and salinity 12-month climatology from the World Ocean Atlas 2018 climatology - WOA2018 -528 https://www.ncei.noaa.gov/archive/accession/NCEI-WOA18. 529 Code availability 530 All data analysis was accomplished using MATLAB and Python software. The Python code used to filter the ADT maps is 531 part of the py-eddy-tracker algorithm (Mason et al., 2014), improved in collaboration between IMEDEA (E. Mason) and CLS, 532 freely available under GNU General Public License (https://github.com/AntSimi/py-eddy-tracker/releases/tag/v3.1.0). The GSW oceanographic toolbox (GSW-OT - www.TEOS-10.org) was used to compute the Conservative Temperature (CT) 533 534 and Absolute Salinity (SA) as well as the mixed layer depth (MLD), and the package http://www.teos-535 10.org/preteos10 software/neutral density.html to compute the neutral isopycnal surfaces.

that most eddy anomalies are generated due to a mechanism of eddy pumping, resulting in warm and saltier (cold and fresher)

# 536 Author contribution

- 537 Conceptualisation: SMSF and AJP. Formal analysis: SMSF. Investigation: SMSF. Methodology: SMSF and AJP. Software:
- 538 SMSF. Supervision: AJL. Validation: SMSF. Visualisation: SMSF. Writing (original draft preparation): SMSF; Writing
- (review and editing): SMSF and AJP

#### 540 Author Disclaimer

The authors declare that they have no conflict of interest.





# 542 Acknowledgements

- 543 The authors would like to thank the Portuguese Fundação para a Ciência e a Tecnologia for funding this work. A special thanks
- 544 to Professor Trevor McDougall, Damien Desbruyères, Ricardo Sanchez Leal, and Ying Zhang for all their help on a deeper
- understanding of the spice and heave concepts and in their computational implementation.

### Financial support

546

- 547 Susana M. Silva-Fernandes is supported by the Portuguese Fundação para a Ciência e a Tecnologia (FCT) through the Doctoral
- Grant PD/BD/142777/2018, within the Earth Systems Doctoral Program of the Faculty of Sciences of the University of Lisbon.
- This work was funded by the Portuguese Fundação para a Ciência e a Tecnologia (FCT) I.P./MCTES through national funds
- 550 (PIDDAC) UIDB/50019/2023 and LA/P/0068/2020 (https://doi.org/10.54499/LA/P/0068/2020), and UID/PRR/50019/2025
- 551 (https://doi.org/10.54499/UID/PRR/50019/2025).

### 552 References

- Alves, M. L. G. R. and De Verdière, A. C.: Instability dynamics of a subtropical jet and applications to the Azores front current
- 554 system: Eddy-driven mean flow, J. Phys. Oceanogr., 29, 837-864, https://doi.org/10.1175/1520-
- 555 0485(1999)029<0837:IDOASJ>2.0.CO;2, 1999.
- 556 Amores, A., Melnichenko, O., and Maximenko, N.: Coherent mesoscale eddies in the North Atlantic subtropical gyre: 3-D
- 557 structure and transport with application to the salinity maximum, J. Geophys. Res. Ocean., 122, 23-41,
- 558 https://doi.org/10.1002/2016JC012256, 2017.
- Barbosa Aguiar, A. C., Peliz, A. J., Cordeiro Pires, A., and Le Cann, B.: Zonal structure of the mean flow and eddies in the
- 560 Azores Current system, J. Geophys. Res. Ocean., 116, 1–14, https://doi.org/10.1029/2010JC006538, 2011.
- 561 Barbosa Aguiar, A. C., Peliz, Á., and Carton, X.: A census of meddies in a long-term high-resolution simulation, Prog.
- 562 Oceanogr., 116, 80–94, https://doi.org/10.1016/j.pocean.2013.06.016, 2013.
- Barnes, S. L.: Mesoscale objective analysis using weighted time-series observations, 657–662, 1973.
- Bashmachnikov, I., Neves, F., Calheiros, T., and Carton, X.: Properties and pathways of Mediterranean water eddies in the
- 565 Atlantic, Prog. Oceanogr., 137, 149–172, https://doi.org/10.1016/j.pocean.2015.06.001, 2015.
- 566 Bindoff, N. L. and Mcdougall, T. J.: Diagnosing Climate Change and Ocean Ventilation Using Hydrographic Data, J. Phys.
- 567 Oceanogr., 24, 1137–1152, https://doi.org/10.1175/1520-0485(1994)024<1137:DCCAOV>2.0.CO;2, 1994.
- 568 Caldeira, R. M. A. and Reis, J. C.: The Azores confluence zone, Front. Mar. Sci., 4, 1-14,
- 569 https://doi.org/10.3389/fmars.2017.00037, 2017.
- 570 Chaigneau, A., Le Texier, M., Eldin, G., Grados, C., and Pizarro, O.: Vertical structure of mesoscale eddies in the eastern
- 571 South Pacific Ocean: A composite analysis from altimetry and Argo profiling floats, J. Geophys. Res. Ocean., 116, 1–16,





- 572 https://doi.org/10.1029/2011JC007134, 2011.
- 573 Chelton, D. B., Schlax, M. G., and Samelson, R. M.: Global observations of nonlinear mesoscale eddies, Prog. Oceanogr., 91,
- 574 167–216, https://doi.org/10.1016/j.pocean.2011.01.002, 2011.
- Desbruyères, D. G., Bravo, E. P., Thierry, V., Mercier, H., Lherminier, P., Cabanes, C., Biló, T. C., Fried, N., and Femke De
- Jong, M.: Warming-to-Cooling Reversal of Overflow-Derived Water Masses in the Irminger Sea During 2002–2021, Geophys.
- 577 Res. Lett., 49, https://doi.org/10.1029/2022GL098057, 2022.
- 578 Dong, C., McWilliams, J. C., Liu, Y., and Chen, D.: Global heat and salt transports by eddy movement, Nat. Commun., 5, 1–
- 579 6, https://doi.org/10.1038/ncomms4294, 2014.
- 580 Frazão, H. C., Prien, R. D., Schulz-bull, D. E., Seidov, D., and Waniek, J. J.: The Forgotten Azores Current: A Long-Term
- 581 Perspective, 9, 1–14, https://doi.org/10.3389/fmars.2022.842251, 2022.
- Frenger, I., Münnich, M., Gruber, N., and Knutti, R.: Southern <scp>O</scp> cean eddy phenomenology, J. Geophys. Res.
- 583 Ocean., 120, 7413–7449, https://doi.org/10.1002/2015JC011047, 2015.
- Gaube, P., Early, J., Chelton, D., Samelson, R., and Schlax, M.: The Influence of Nonlinear Mesoscale Eddies on Oceanic
- 585 Chlorophyll, 9569–9569 pp., 2011.
- Gaube, P., McGillicuddy, D. J., Chelton, D. B., Behrenfeld, M. J., and Strutton, P. G.: Regional variations in the influence of
- 587 mesoscale eddies on near-surface chlorophyll, J. Geophys. Res. Ocean., 119, 8195-8220,
- 588 https://doi.org/10.1002/2014JC010111, 2014.
- Gould, W. J.: Physical Oceanography of the Azores Front, 14, 167–190, https://doi.org/https://doi.org/10.1016/0079-
- 590 6611(85)90010-2, 1985.
- Han, L. and Yan, X. H.: Warming in the Agulhas Region during the Global Surface Warming Acceleration and Slowdown,
- 592 Sci. Rep., 8, 1–7, https://doi.org/10.1038/s41598-018-31755-1, 2018.
- 593 He, Q., Zhan, W., Cai, S., Du, Y., Chen, Z., Tang, S., and Zhan, H.: Enhancing impacts of mesoscale eddies on Southern
- Ocean temperature variability and extremes, Proc. Natl. Acad. Sci., 120, 2017, https://doi.org/10.1073/pnas.2302292120,
- 595 2023.
- He, Q., Mo, D., Zhan, W., Cai, S., Tang, S., Zha, G., and Zhan, H.: Thermal Imprints of Mesoscale Eddies in the Global Ocean,
- J. Phys. Oceanogr., 54, 1991–2009, https://doi.org/10.1175/JPO-D-23-0226.1, 2024.
- Jackett, D. R. and Mcdougall, T. J.: A neutral density variable for the world's oceans, J. Phys. Oceanogr., 27, 237–263,
- 599 https://doi.org/10.1175/1520-0485(1997)027<0237:ANDVFT>2.0.CO;2, 1997.
- Juliano, M. F. and Alves, M. L. G. R.: The atlantic subtropical front/current systems of Azores and St. Helena, J. Phys.
- 601 Oceanogr., 37, 2573–2598, https://doi.org/10.1175/2007JPO3150.1, 2007.
- 602 Keppler, L., Cravatte, S., Chaigneau, A., Pegliasco, C., Gourdeau, L., and Singh, A.: Observed Characteristics and Vertical
- 603 Structure of Mesoscale Eddies in the Southwest Tropical Pacific, J. Geophys. Res. Ocean., 123, 2731–2756,
- 604 https://doi.org/10.1002/2017JC013712, 2018.
- Keppler, L., Eddebbar, Y. A., Gille, S. T., Guisewhite, N., Mazloff, M. R., Tamsitt, V., Verdy, A., and Talley, L. D.: Effects





- of Mesoscale Eddies on Southern Ocean Biogeochemistry, AGU Adv., 5, https://doi.org/10.1029/2024AV001355, 2024.
- 607 Klein, B. and Siedler, G.: On the origin of the Azores Current, J. Geophys. Res. Ocean., 94, 6159-6168,
- 608 https://doi.org/10.1029/jc094ic05p06159, 1989.
- Mahadevan, A.: The Impact of Submesoscale Physics on Primary Productivity of Plankton, Ann. Rev. Mar. Sci., 8, 161–184,
- 610 https://doi.org/10.1146/annurev-marine-010814-015912, 2016.
- Martin, A. P. and Richards, K. J.: Mechanisms for vertical nutrient transport within a North Atlantic mesoscale eddy, Deep.
- 612 Res. Part II Top. Stud. Oceanogr., 48, 757–773, https://doi.org/10.1016/S0967-0645(00)00096-5, 2001.
- Mason, E., Pascual, A., and McWilliams, J. C.: A new sea surface height-based code for oceanic mesoscale eddy tracking, J.
- Atmos. Ocean. Technol., 31, 1181–1188, https://doi.org/10.1175/JTECH-D-14-00019.1, 2014.
- 615 McGillicuddy, D. J.: Mechanisms of Physical-Biological-Biogeochemical Interaction at the Oceanic Mesoscale, 125–159 pp.,
- 616 https://doi.org/10.1146/annurev-marine-010814-015606, 2016.
- Mourino, B., Fernández, E., Etienne, H., Hernández, F., and Giraud, S.: Significance of cyclonic SubTropical Oceanic Rings
- of Magnitude (STORM) eddies for the carbon budget of the euphotic layer in the subtropical northeast Atlantic, J. Geophys.
- Res. Ocean., 108, https://doi.org/10.1029/2003jc001884, 2003.
- Mouriño, B., Fernández, E., Escánez, J., de Armas, D., Giraud, S., Sinha, B., and Pingree, R.: A Subtropical Oceanic Ring of
- Magnitude (STORM) in the Eastern North Atlantic: physical, chemical and biological properties, Deep Sea Res. Part II Top.
- 622 Stud. Oceanogr., 49, 4003–4021, https://doi.org/10.1016/S0967-0645(02)00139-X, 2002.
- 623 Ollitrault, M. and Colin de Verdière, A.: SOFAR Floats Reveal Midlatitude Intermediate North Atlantic General Circulation.
- 624 Part I: A Lagrangian Descriptive View, J. Phys. Oceanogr., 32, 2020-2033, https://doi.org/10.1175/1520-
- 625 0485(2002)032<2020:SFRMIN>2.0.CO;2, 2002.
- 626 Pegliasco, C., Chaigneau, A., and Morrow, R.: Main eddy vertical structures observed in the four major Eastern Boundary
- 627 Upwelling Systems, J. Geophys. Res. Ocean., 120, 6008–6033, https://doi.org/10.1002/2015JC010950, 2015.
- Pingree, R.: Ocean structure and climate (Eastern North Atlantic): In situ measurement and remote sensing (altimeter), J. Mar.
- 629 Biol. Assoc. United Kingdom, 82, 681–707, https://doi.org/10.1017/S0025315402006082, 2002.
- Pingree, R. D. and Sinha, B.: Dynamic topography (ERS-1/2 and seatruth) of Subtropical Ring (STORM 0) in the storm
- 631 corridor (32-34°N, Eastern Basin, North Atlantic Ocean), J. Mar. Biol. Assoc. United Kingdom, 78, 351-376,
- 632 https://doi.org/10.1017/S0025315400041503, 1998.
- 633 Pingree, R. D., Sinha, B., New, A. L., Waddington, I., Head, R. N., and Nechvolodov, L. V.: Will deep subtropical ring "Storm
- Physalia" cross the mid Atlantic ridge and reach America?, J. Mar. Biol. Assoc. United Kingdom, 76, 553-567,
- 635 https://doi.org/10.1017/s0025315400031271, 1996.
- Richardson, P. L., McCartney, M. S., and Maillard, C.: A search for meddies in historical data, Dyn. Atmos. Ocean., 15, 241-
- 637 265, https://doi.org/10.1016/0377-0265(91)90022-8, 1991.
- Richardson, P. L., Bower, A. S., and Zenk, W.: A census of Meddies tracked by floats, Prog. Oceanogr., 45, 209-250,
- 639 https://doi.org/10.1016/S0079-6611(99)00053-1, 2000.





- Sangrà, P., Pascual, A., Rodríguez-Santana, Á., Machín, F., Mason, E., McWilliams, J. C., Pelegrí, J. L., Dong, C., Rubio, A.,
- Arístegui, J., Marrero-Díaz, Á., Hernández-Guerra, A., Martínez-Marrero, A., and Auladell, M.: The Canary Eddy Corridor:
- A major pathway for long-lived eddies in the subtropical North Atlantic, Deep. Res. Part I Oceanogr. Res. Pap., 56, 2100-
- 643 2114, https://doi.org/10.1016/j.dsr.2009.08.008, 2009.
- 644 Silva-Fernandes, S. M. and Peliz, A. J.: The Turbulent Structure of the Azores Current System: A Statistical Analysis, J.
- Geophys. Res. Ocean., 125, 1–19, https://doi.org/10.1029/2020JC016327, 2020.
- Treguier, A. M., Deshayes, J., Lique, C., Dussin, R., and Molines, J. M.: Eddy contributions to the meridional transport of salt
- in the North Atlantic, J. Geophys. Res. Ocean., 117, 1–19, https://doi.org/10.1029/2012JC007927, 2012.
- Zhang, W. and Yan, X.-H.: The Subpolar North Atlantic Ocean Heat Content Variability and its Decomposition, Sci. Rep., 7,
- 649 13748, https://doi.org/10.1038/s41598-017-14158-6, 2017.